

## SUPPORTING INFORMATION

---

# **Bottlebrush Polymer Patches Template Heterometal Growth on Gold Nanoparticle Surface**

Minjun Kim<sup>†</sup>, Jiyun Nam<sup>†</sup>, Jiseok Kim, Hyunsik Hwang, Myungeun Seo<sup>\*</sup>, Hyunjoon Song<sup>\*</sup>

Department of Chemistry, Korea Advanced Institute of Science and Technology (KAIST),  
Daejeon 34141, Republic of Korea

E-mail: seomyungeun@kaist.ac.kr, hsong@kaist.ac.kr

## SUPPORTING INFORMATION

### Materials

Gold(III) chloride hydrate ( $\text{HAuCl}_4 \cdot x\text{H}_2\text{O}$ , 99.995%), trisodium citrate dihydrate (SC, USP testing specifications), silver nitrate ( $\text{AgNO}_3$ , ACS reagent,  $\geq 99.0\%$ ), chloroplatinic acid hydrate ( $\text{H}_2\text{PtCl}_6 \cdot x\text{H}_2\text{O}$ ,  $\geq 99.9\%$ ), polyvinylpyrrolidone (PVP,  $M_w \sim 55,000$ ), 4-dimethylaminopyridine (DMAP,  $\geq 99\%$ ), cis-5-norbornene-exo-2,3-dicarboxylic anhydride ( $\geq 99\%$ ), triethylamine ( $\geq 99\%$ ), norbornene ( $\geq 99\%$ ), sodium azide ( $\geq 99.5\%$ ), 4-pentynoic acid (95%), styrene ( $\geq 99\%$ ), copper(I) bromide (98%), methyl  $\alpha$ -bromoisobutyrate ( $\geq 99\%$ ), N,N,N',N'',N'''-pentamethyldiethylenetriamine (99%), 1-dodecanethiol ( $\geq 98\%$ ), carbon disulfide ( $\geq 99\%$ ), and ethyl vinyl ether ( $\geq 99\%$ ) were purchased from Sigma-Aldrich. Hydrazine monohydrate (HZ,  $> 98.0\%$ ), N-(3-dimethylaminopropyl)-N'-ethylcarbodiimide hydrochloride (EDC), tricapyrylmethyl ammonium chloride, and 8-aminooctanol ( $\geq 98\%$ ) were purchased from Tokyo Chemical Industry (Tokyo, Japan). Grubbs third generation catalysts (G3) were donated by Materia, Inc. According to the literature, the linear PS carrying the TTC group at the chain end ( $M_n = 25 \text{ kg mol}^{-1}$ ,  $\mathcal{D} = 1.51$ ) was synthesized through reversible addition-fragmentation chain transfer (RAFT) polymerization.<sup>1</sup> Poly(styrene),  $\omega$ -thiol-terminated ( $M_n = 104.5 \text{ kg mol}^{-1}$ ,  $\mathcal{D} = 1.11$ ) was purchased from Polymer Source, inc. Other laboratory chemicals used in work-up processes were purchased from Daejung. HPLC grade dimethylformamide (DMF), toluene, chloroform ( $\text{CHCl}_3$ ), tetrahydrofuran (THF), and dichloromethane (DCM) were purchased from Burdick & Jackson. Uranyl acetate ( $\geq 98\%$ ) was purchased from SPI Supplies.

### Characterization

The nanostructures were characterized by transmission electron microscopy (TEM, FEI Tecnai TF30 ST, 300 kV), scanning tunneling electron microscope-energy dispersive spectroscopy (STEM-EDS), and scanning electron microscopy (SEM, Field Emission SEM (JSM-IT800)). The samples were prepared by dropping the sample dispersion to the TEM grid (carbon-coated 300 mesh copper grids, TED PELLA Inc.). Then, filter paper was used to wick off the excess dispersion, followed by drying in air. Uranyl acetate was used as a negative staining agent. Dynamic light scattering (DLS) and zeta potential measurements were performed on a Nanobrook Omni (Holtsville, NY) equipped with a 35 mW He-Ne laser at the wavelength of 640 nm with a scattering angle of  $90^\circ$ . Samples were prepared at a concentration of  $0.5 \text{ mg mL}^{-1}$  and filtered through  $0.2 \mu\text{m}$  PTFE syringe filters before the measurement. Then, the hydrodynamic diameter ( $D_h$ ) was analyzed by DLS, and zeta potential was measured using a phase analysis light scattering (PALS) mode. The absorbances of Au NPs and polymers were characterized by UV-3600 UV-vis spectroscopy. The samples were prepared in the micro-quartz

## SUPPORTING INFORMATION

---

cell (path length = 10 mm, iNexus Inc.).  $^1\text{H}$  NMR spectroscopy was conducted on a Bruker Avance 400 MHz spectrometer (Billerica, MA) in  $\text{CDCl}_3$  using the residual NMR solvent signal as an internal reference at 7.26 ppm. The size exclusion chromatography (SEC) system was equipped with a 1260 refractive index detector (Santa Barbara, CA) and PSS GRAM analytical 10000 Å columns. DMF was used as an eluent at 45 °C, and the number-average molar mass ( $M_{n, \text{SEC}}$ ) of the polymers was calculated relative to the linear polystyrene standards (EasiCal) purchased from Agilent Technologies. Preparative SEC was conducted on a LaboACE LC-5060 (Tokyo, Japan) with JAIGEL-4 and 3HR column using an RI-700 LA refractive index detector. Chloroform was used as an eluent at 25 °C with a flow rate of 10  $\text{mL min}^{-1}$ . The composition of BBCP-Au was confirmed using thermogravimetric analysis (TGA, TG209 F1 Libra, Netzsch, Germany) at a heating rate of 10 °C  $\text{min}^{-1}$  under the nitrogen flow of 20  $\text{mL min}^{-1}$ .

# SUPPORTING INFORMATION

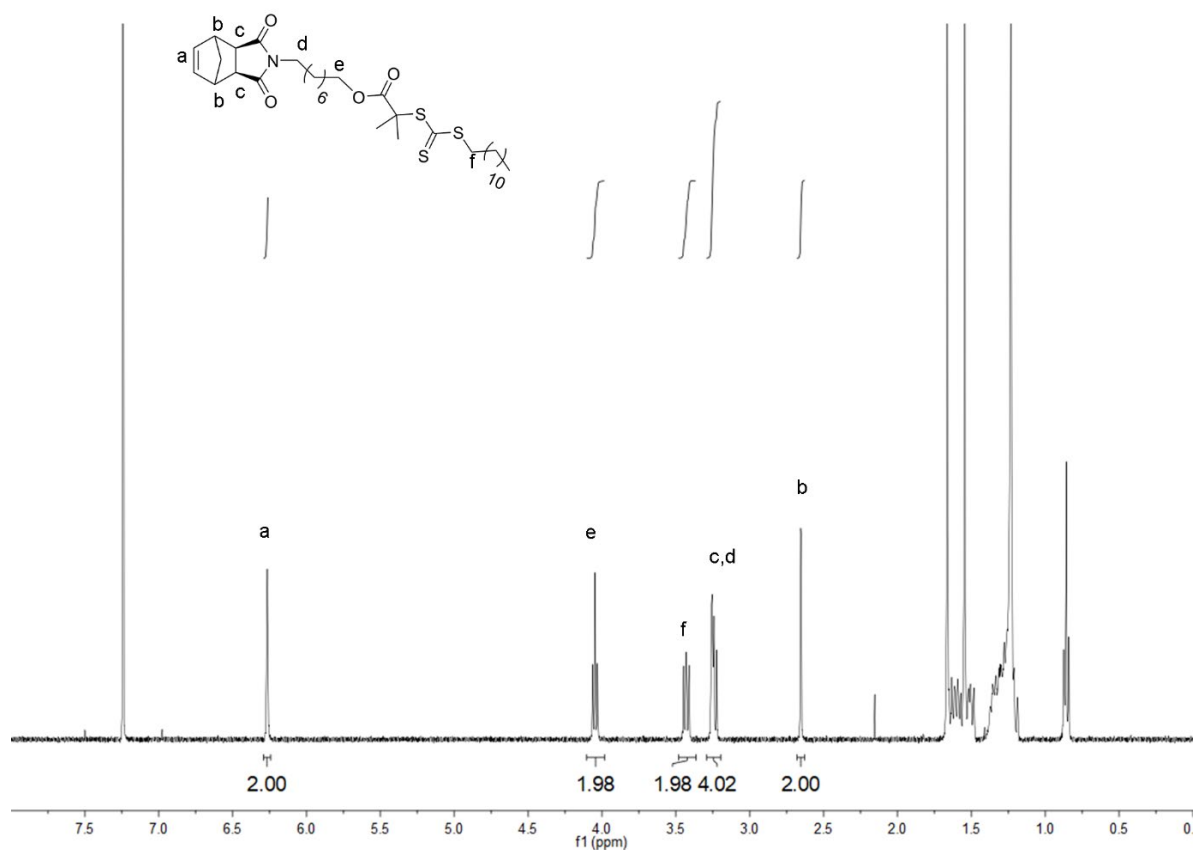


**Fig. S1**  $^1\text{H}$  NMR spectrum of TTC-N (400 MHz,  $\text{CDCl}_3$ ).

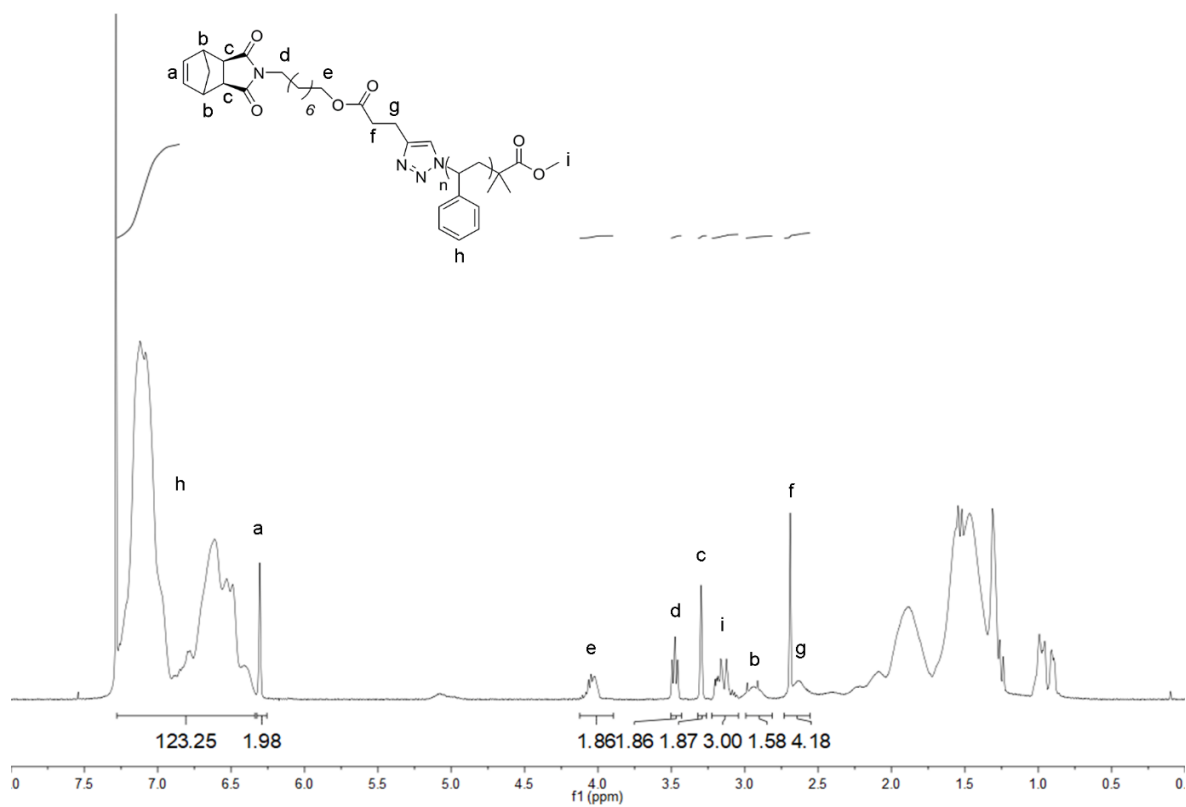
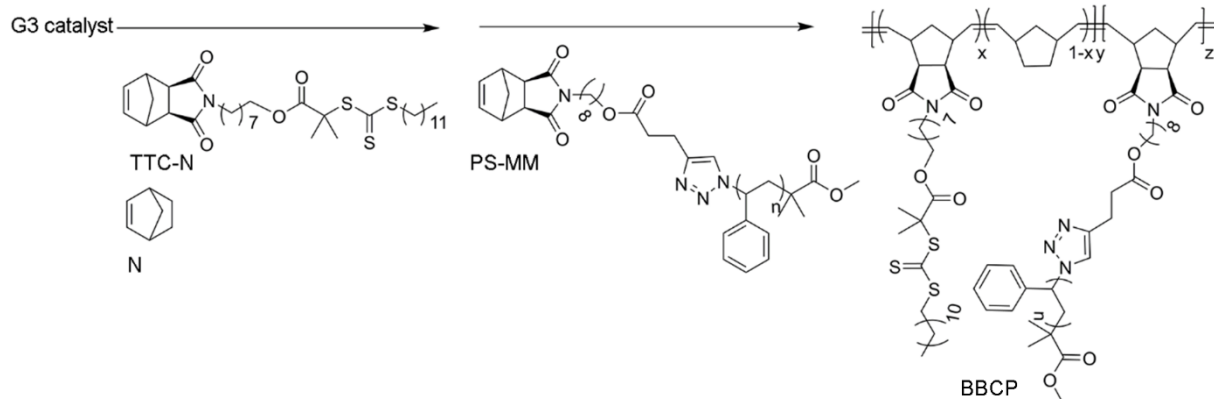


**Fig. S2**  $^1\text{H}$  NMR spectrum of PS-MM (400 MHz,  $\text{CDCl}_3$ ).



**Scheme S1** Synthesis of BBCP.

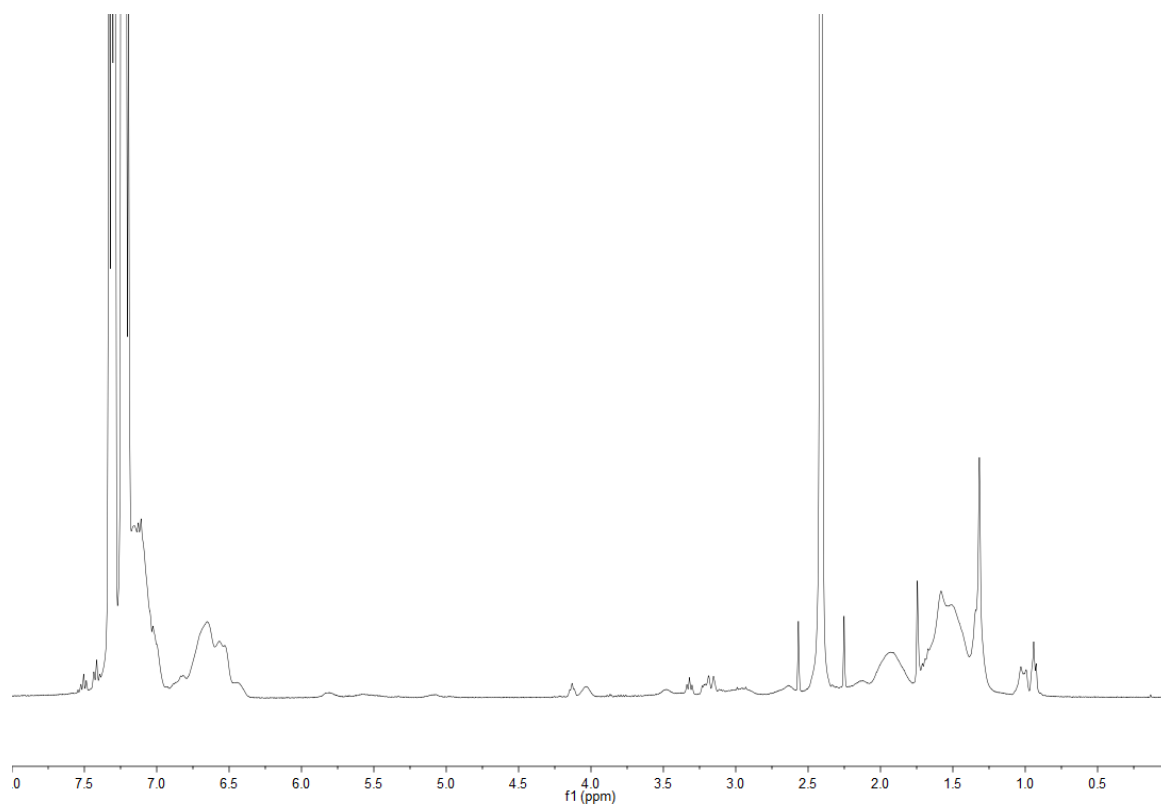


**Fig. S3**  $^1\text{H}$  NMR spectrum of the crude polymerization mixture of BBCP (400 MHz,  $\text{CDCl}_3$ ).

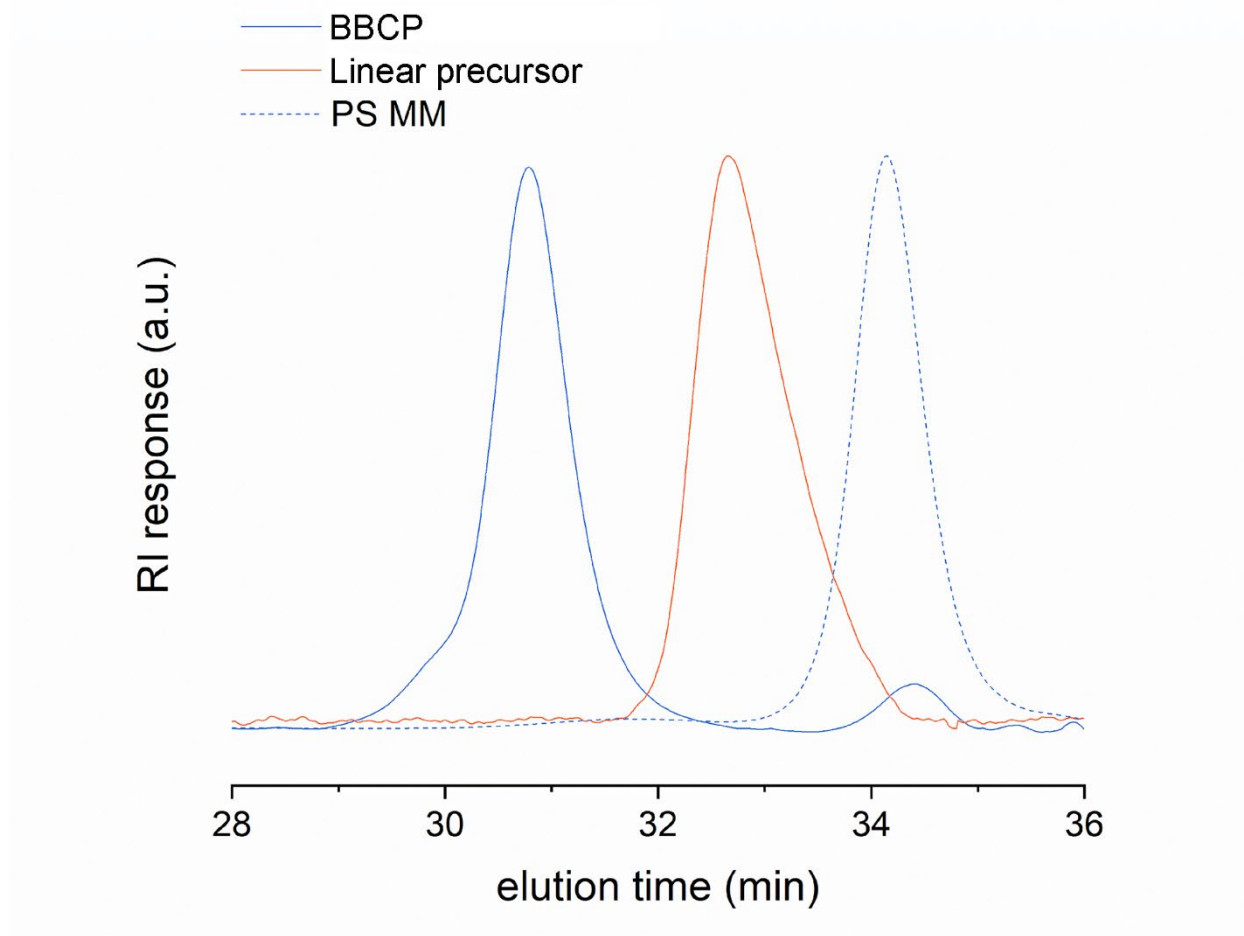


**Fig. S4** SEC traces of BBCP and the corresponding precursor. PS-MM is shown as a dashed line for reference.

## SUPPORTING INFORMATION

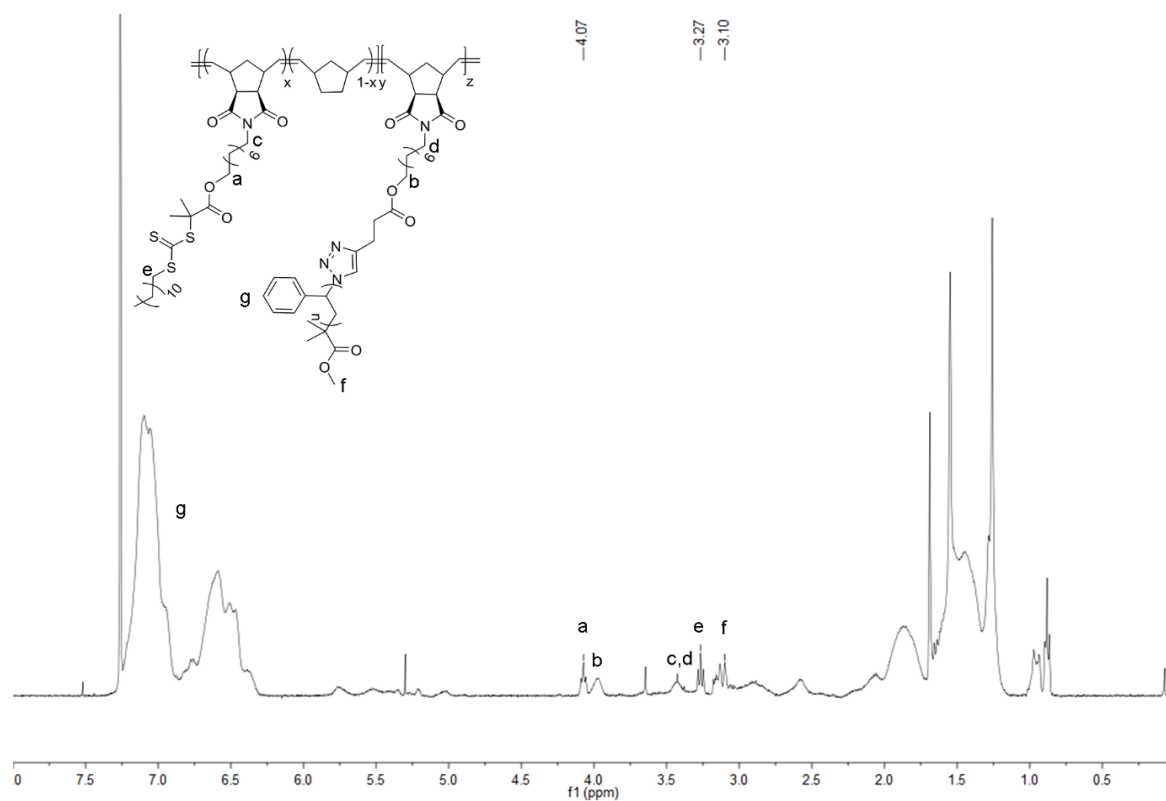


**Fig. S5**  $^1\text{H}$  NMR spectrum of BBCP (400 MHz,  $\text{CDCl}_3$ ).

**Table S1** Characterization of BBCP and PS-MM

Entry	Conv. (%) <sup>[a]</sup>	$M_{n,\text{NMR}}$ ( $\text{kg mol}^{-1}$ )	$M_{n,\text{theo}}$ <sup>[b]</sup> ( $\text{kg mol}^{-1}$ )	$M_{n,\text{SEC}}$ <sup>[c]</sup> ( $\text{kg mol}^{-1}$ )	$\bar{D}$ <sup>[c]</sup>
PS-MM	-	2.7	-	-	1.23
BBCP	93	-	460.8	232.4	1.37

[a] Determined by comparing the peak area of BBCP and residual PS-MM in the SEC trace

[b]  $M_{n,\text{theo}} = \text{MW of N} \times [\text{N/Ru}] + \text{MW of TTC-N} \times [\text{TTC-N/Ru}] + M_{n,\text{NMR}} \text{ of PS-MM} \times [\text{PS-MM/Ru}] \times \text{Conversion}$ .

[c] Determined by DMF-SEC with a RI detector based on linear PS standards

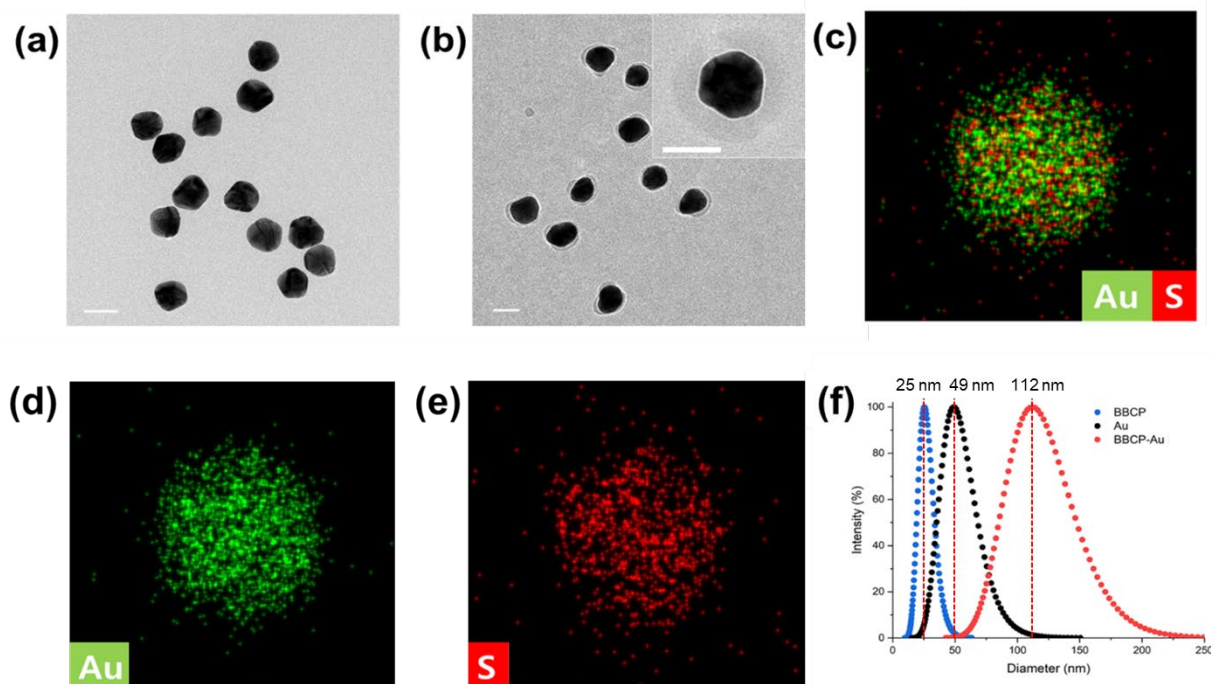


**Fig. S6** TEM images of (a) citrate-stabilized Au NPs and (b) BBCP-Au. STEM-EDS elemental mapping images of (c) Au and S, (d) Au, and (e) S in BBCP-Au. (f) Lognormal distribution of citrate-Au in water (black), BBCP in chloroform (blue), and BBCP-Au dispersion in chloroform (red) obtained by DLS analysis. The scale bars represent 50 nm.

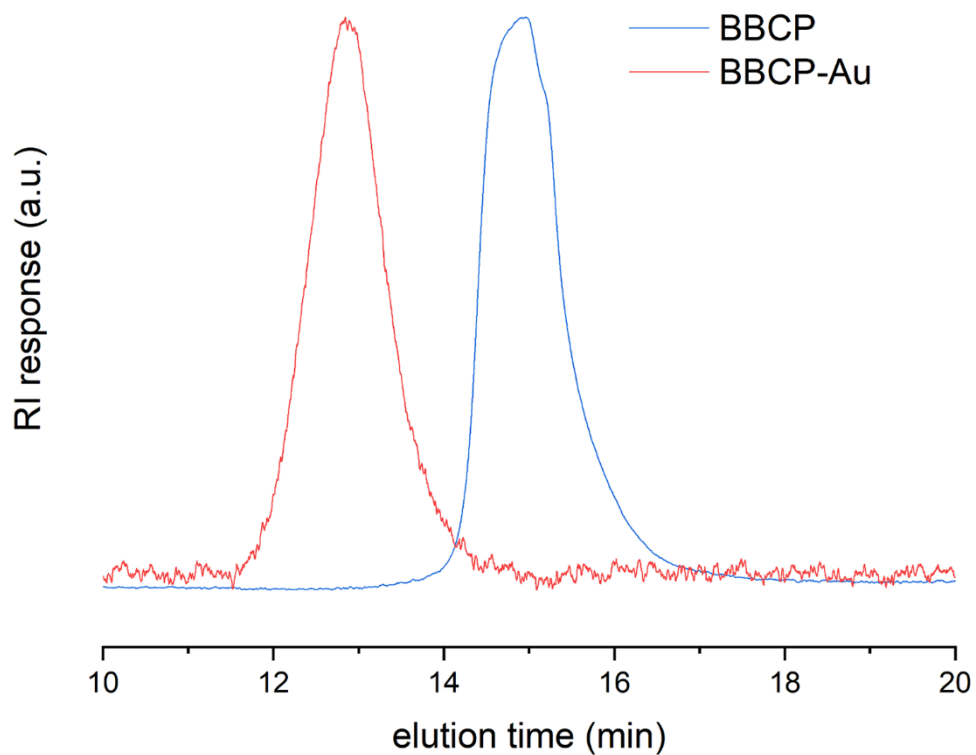


**Fig. S7** Preparative SEC traces of BBCP-Au and BBCP.

**Table S2** Zeta potential and mobility of BBCP-Au and citrate-Au NPs.

	<b>Zeta potential (mV)</b>	<b>Mobility (<math>\mu\text{s}/(\text{V}/\text{cm})</math>)</b>
<b>BBCP-Au</b>	-3.93	-0.16
<b>Citrate-Au NPs</b>	-19.81	-0.83

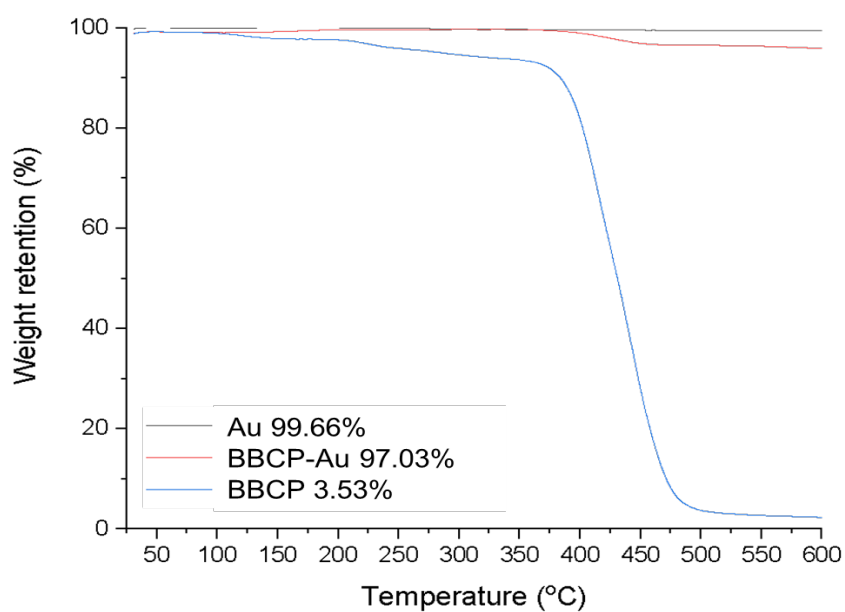


**Fig. S8** TGA measurements of citrate-capped Au NPs, BBCP-Au, and BBCP.

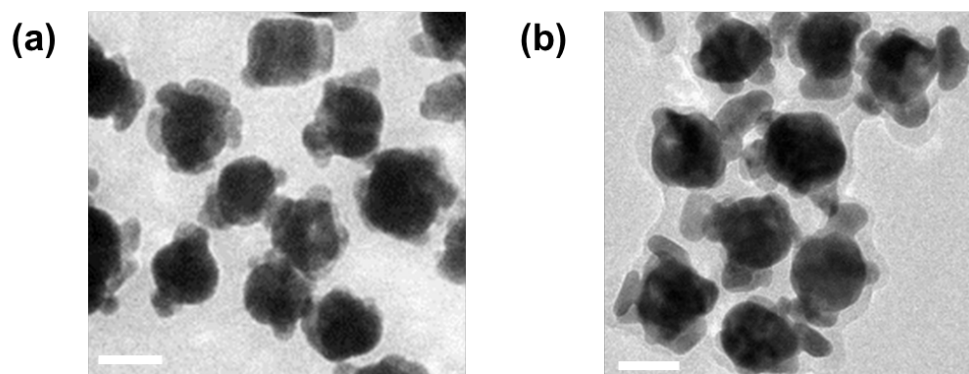


**Fig. S9** TEM images of multiple island formations after (a) 20 min and (b) 3 months incubation times of BBCP-Au with 30% of the water content. The scale bars are 50 nm.

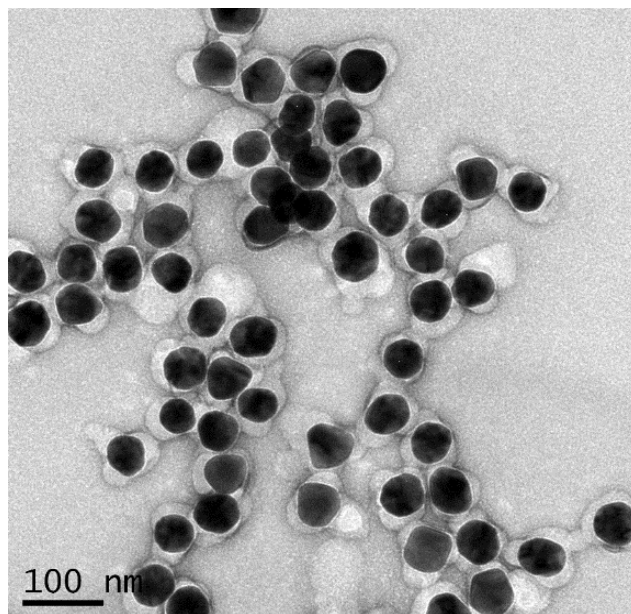


**Fig. S10** A **wide-view** TEM image of multiple islands corresponding to Fig. 1a after negative staining.

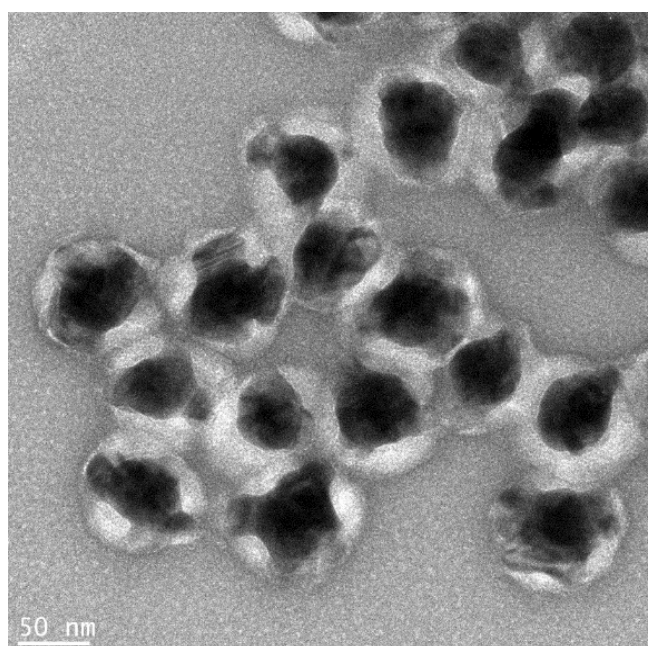


**Fig. S11** A **wide-view** TEM image of multiple islands corresponding to Fig. 1b after negative staining.

## SUPPORTING INFORMATION

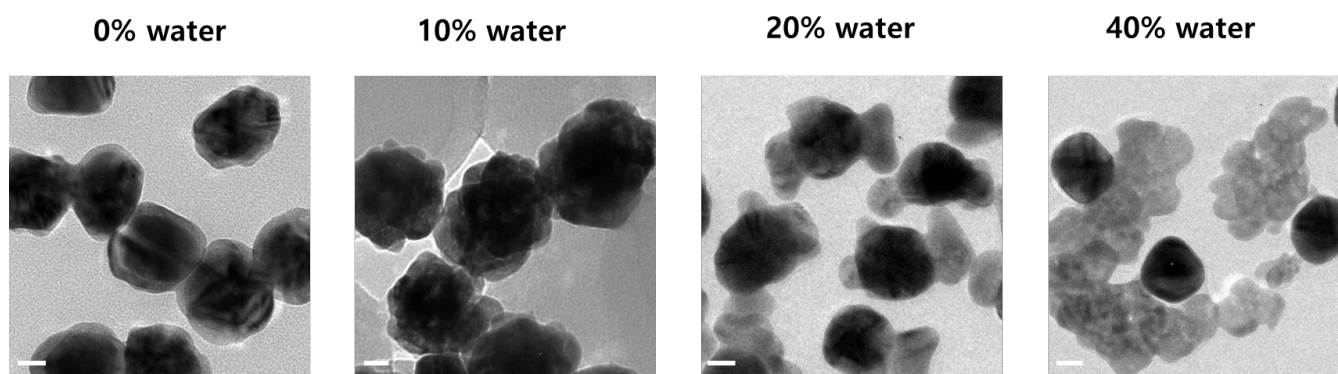


**Fig. S12** TEM images of Au-Ag heterostructures using BBCP containing 320 norbornene units of the brush backbone. The scale bars are 20 nm.

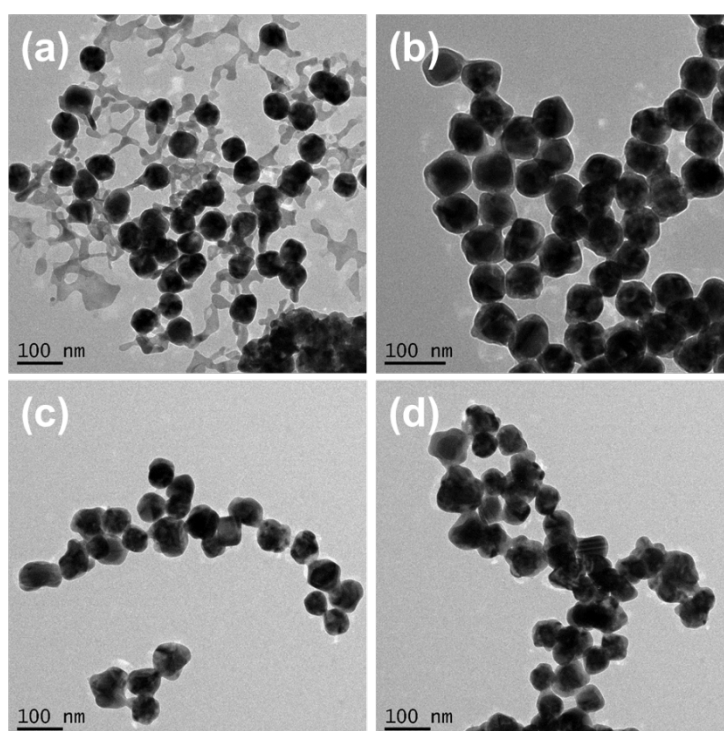


**Fig. S13** TEM images of (PS-SH)-capped Au NPs after Ag deposition. The water percentages in DMF were (a) 0 vol %, (b) 10 vol %, (c) 30 vol %, and (d) 50 vol%.

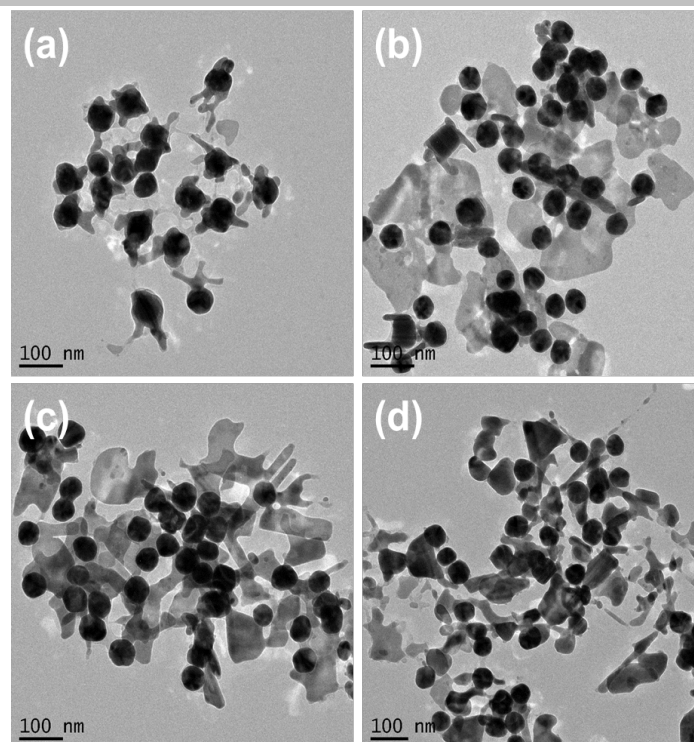


**Fig. S14** TEM images of (PS-TTC)-capped Au NPs after Ag deposition. The water percentages in DMF were (a) 0 vol %, (b) 10 vol %, (c) 30 vol %, and (d) 50 vol%.

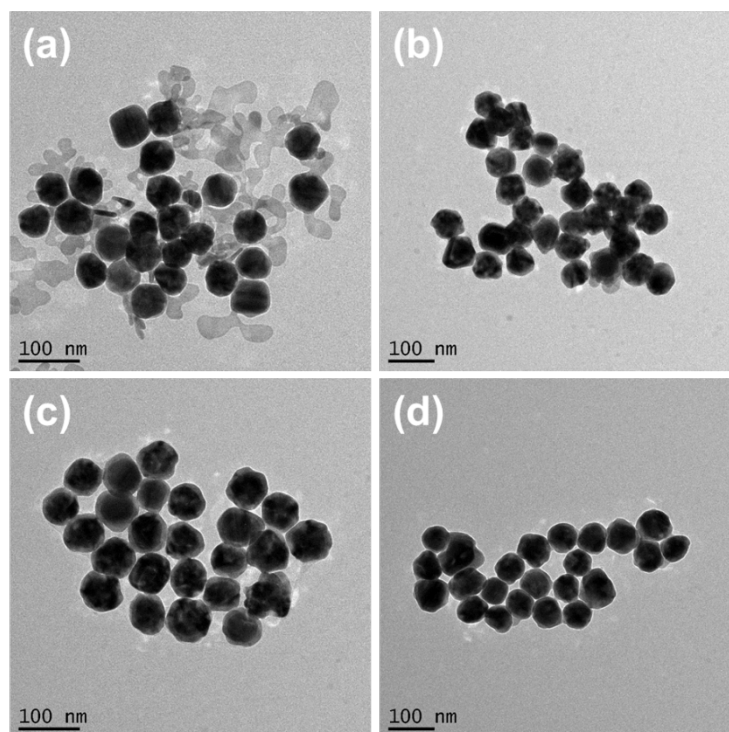
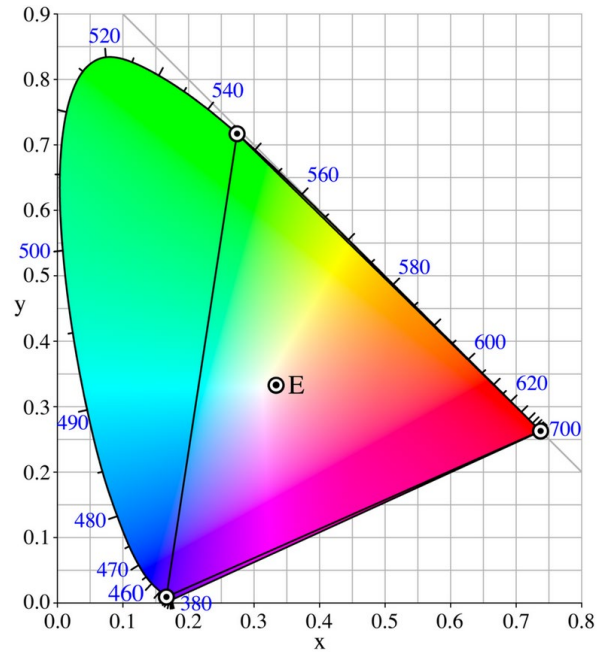


**Fig. S15** TEM images of PVP-capped Au NPs after Ag deposition. The water percentages in DMF were (a) 0 vol %, (b) 10 vol %, (c) 30 vol %, and (d) 50 vol%.

## SUPPORTING INFORMATION

### Converting process of RGB Information to the Maximum Peak Wavelength.

The converting process uses the color information captured by a dark-field microscope and extracted the maximum scattering peak wavelength.



$$I = VR * 0.299 + VG * 0.5876 + VB * 0.114 \quad (1)$$

$$X = 0.412R + 0.358G + 0.180B \quad (2)$$

$$Y = 0.213R + 0.715G + 0.072B \quad (3)$$

$$Z = 0.019R + 0.119G + 0.950B \quad (4)$$

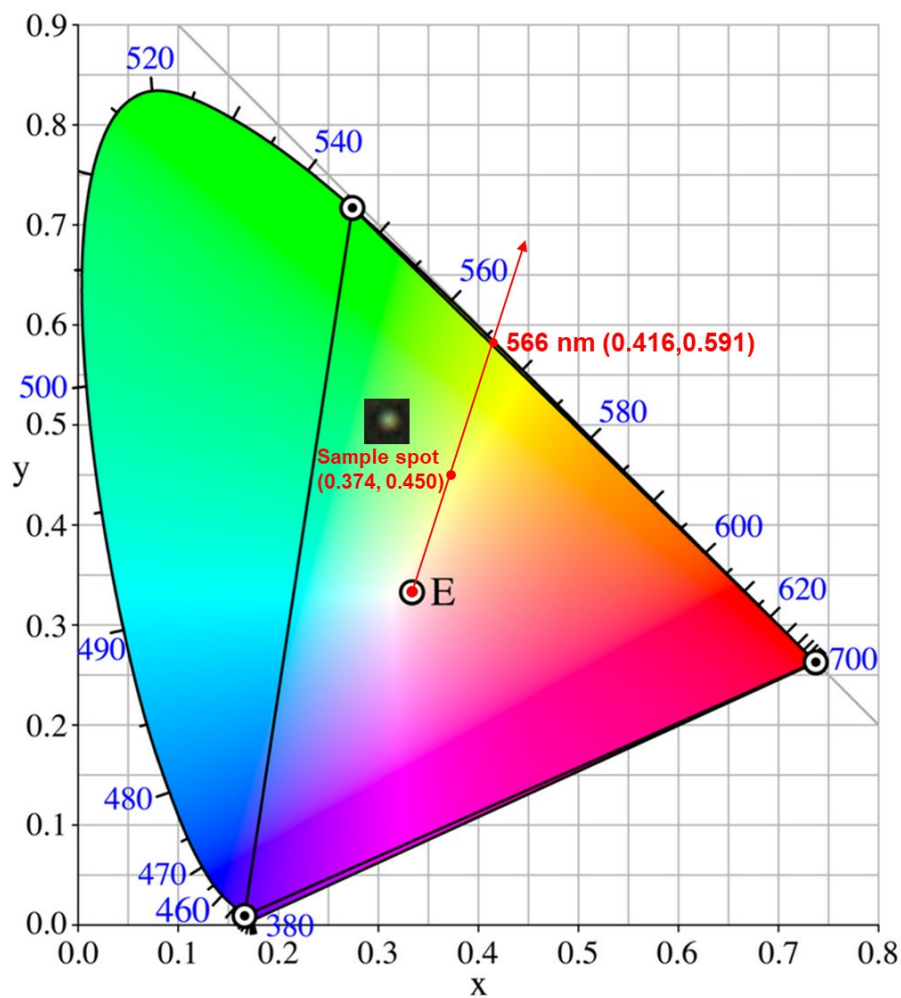
$$x = X/(X + Y + Z) \quad (5)$$

$$y = Y/(X + Y + Z) \quad (6)$$

A Matlab program is utilized to convert the RGB information (VR, VG, VB) obtained from the darkfield image into the scattering light  $\lambda_{\max}$ . The RGB information is extracted from all pixels in an individual particle, and then the intensities are calculated according to equation (1). Among the pixels, the RGB value of the brightest pixel is converted to the x and y values by the equation (2-6). The x and y values are the coordinates of the CIE1931 chromaticity diagram. The achromatic point (E) is defined where  $x = y = 1/3$ . The outer curved boundary of the diagram represents a monochromatic locus. The representative wavelength is determined by extending a straight line from E to (x, y). The intersection of this line with the boundary of the chromaticity diagram corresponds to the wavelength of the peak maximum ( $\lambda_{\max}$ ).<sup>2,3</sup>

## SUPPORTING INFORMATION

As an example, a selected pixel of the sample with the RGB information of (225, 255, 60) was converted to  $(x, y) = (0.374, 0.450)$ . By drawing a line from E to this point, the intersection with the boundary of color space occurred at  $(0.416, 0.591)$ , corresponding to a representative  $\lambda_{\max}$  of 566 nm (see the figure).



## SUPPORTING INFORMATION

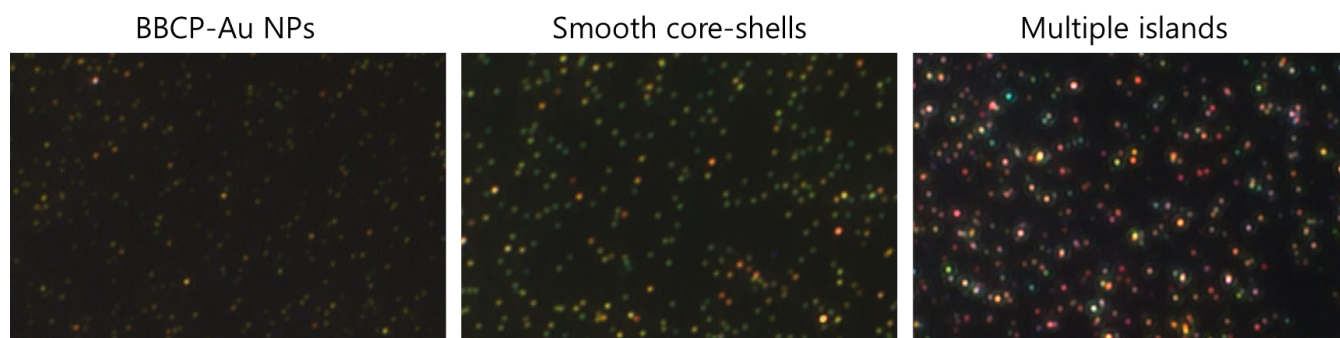


**Fig. S16** Plasmon scattering images of individual NPs using single-particle scatterometry with dark-field microscopy.

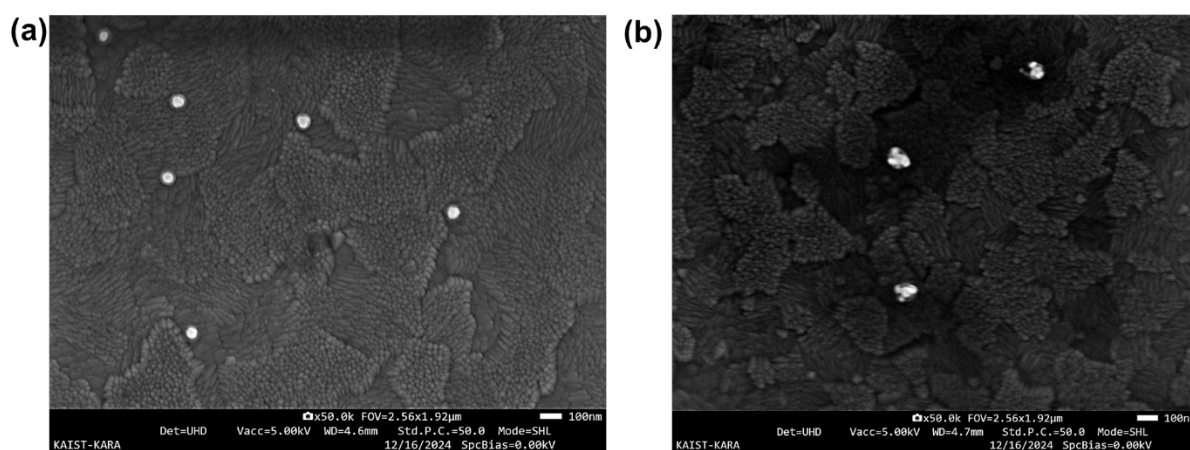
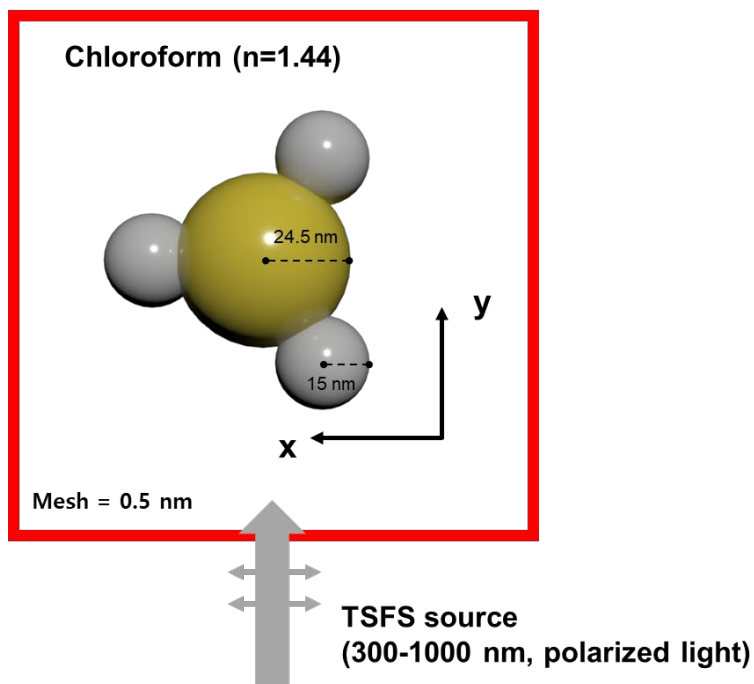


**Fig. S17** SEM images of (a) BBCP-Au and (b) Au-Ag multiple-island particles on ITO-coated glass.

(a)



(b)

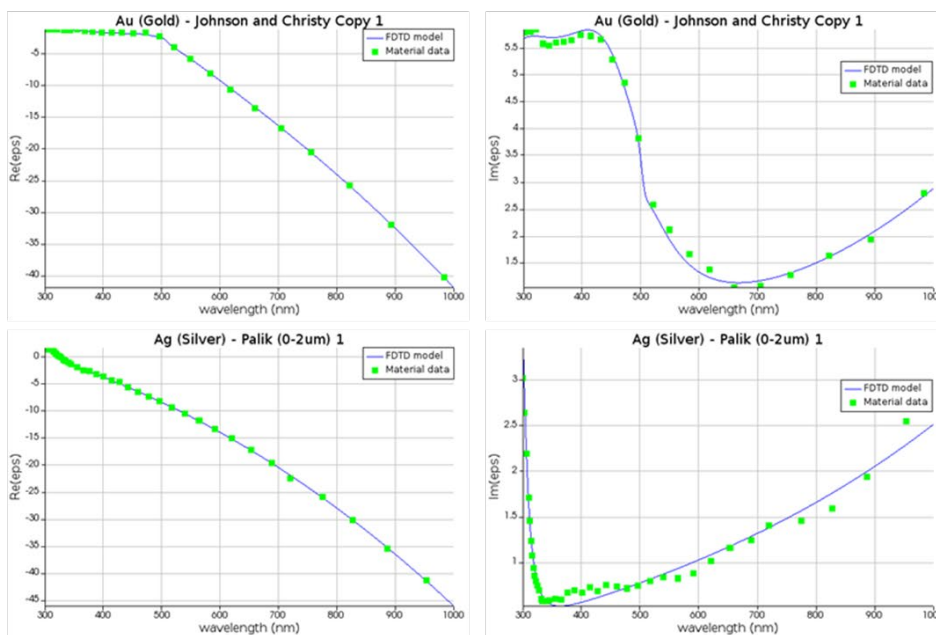


**Fig. S18** (a) A model structure of a single multiple island for FDTD simulation. (b) Materials fitting data ( $\text{Re}(\epsilon)$  and  $\text{Im}(\epsilon)$ ) of gold and silver.

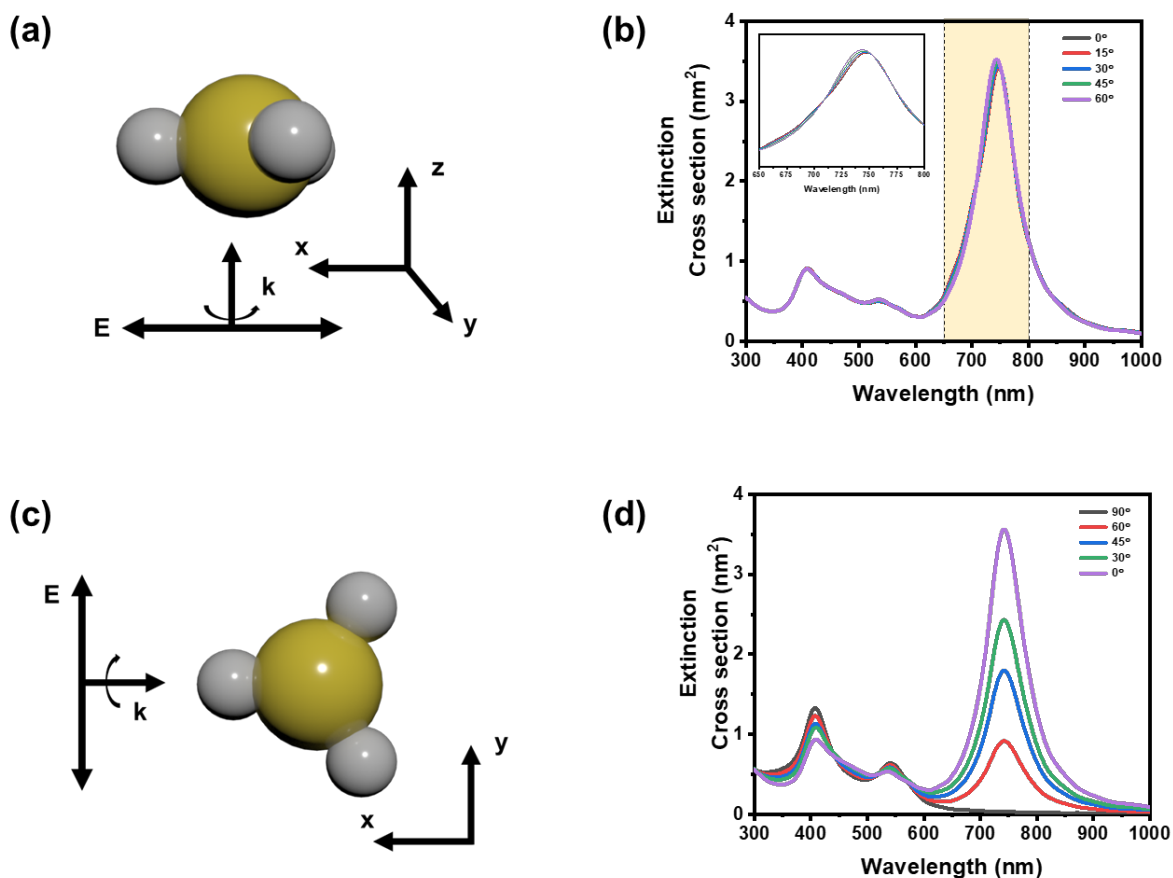


**Fig. S19** (a) An individual multiple-island model where the beam propagation was parallel to the symmetry axis (z) and (b) its simulated extinction cross-section based on the incidence angle of polarized light. (c) The ideal model identical to (a) where the beam propagation was normal to the symmetry axis (z) and (d) its simulated extinction cross-section based on the incidence angle of polarized light.

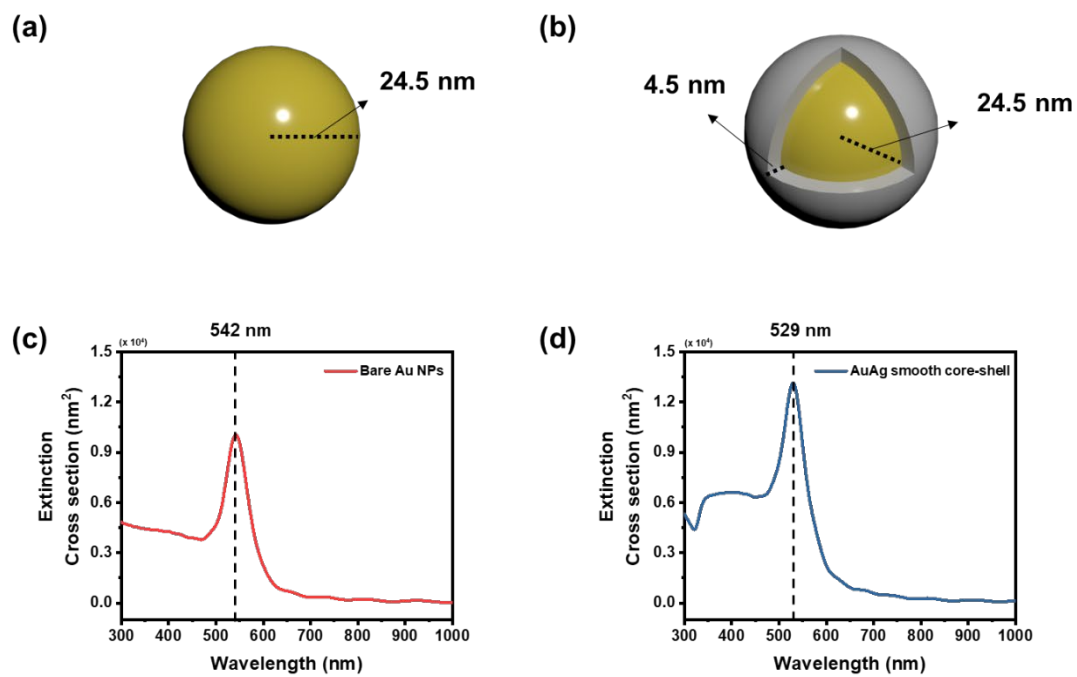


**Fig. S20** Individual model structures of (a) Au sphere and (b) Au-Ag smooth core-shell. Simulated extinction cross-sections of (c) Au sphere and (d) Au-Ag smooth core-shell.

## SUPPORTING INFORMATION

---

### References

- 1 J. T. Lai, D. Filla and R. Shea, *Macromolecules*, 2002, **35**, 6754–6756.
- 2 Y. Park, H. Oh, J. Park, W. Choi, H. Ryu, D. Seo and H. Song, *J. Phys. Chem. C*, 2019, **123**, 23113-23123.
- 3 J. Hao, B. Xiong, X. Cheng, Y. He and E. S. Yeung, *Anal. Chem.*, 2014, **86**, 4663-4667.